nature communications

Article

https://doi.org/10.1038/s41467-026-76918-1

Intelligent artificial olfactory nervous system with sensory adaptation capabilities

Received: 5 April 2024

Accepted: 10 August 2026

Published online: 20 August 2026

Check for updates

Gyuweon Jung[1,2], Jaehyeon Kim[1], Kangwook Choi[1], Hunhee Shin[1], Kwon Dongseok[3], Wonjun Shin[4], Jinwoo Park[1], Donghee Kim[1], Jangsaeng Kim[5], Ryun-Han Koo[1], Woo Young Choi[1] & Jong-Ho Lee[1,3]

Accurate gas identification across diverse environments is crucial for the advancement of intelligent artificial olfaction, but remains challenging for conventional data-driven learning approaches. Here, we report an artificial olfactory nervous system capable of reliably identifying novel gas stimuli regardless of environmental variations by leveraging sensory adaptation mechanisms inspired by biological olfactory systems. Inspired by biological olfactory systems, our system effectively integrates artificial olfactory receptor neurons, cortical neurons, and intermediate olfactory neurons that facilitate signal transmission. Receptor neurons can dynamically adapt their sensitivity to olfactory stimuli, enabling rapid responses to familiar gases and selective filtering of background interference, thus generating distinctive signal patterns for novel gases. Signals from receptor neurons are modulated in olfactory neurons, then fed into the cortical neurons and translated into olfactory perception. We show that, despite being trained in limited settings, the system can accurately identify gases in various environments.

The biological olfactory nervous system (BONS) plays an indispensable role in the evolution and survival of organisms. The BONS enables organisms to respond to and adapt to olfactory stimuli. The system consists of olfactory receptor neurons, olfactory neurons between the receptor and the olfactory cortex, and cortical neurons (Fig. 1a)[1–3]. Receptor neurons are responsible for sensing stimuli, and cortical neurons interpret these stimuli. Olfactory neurons, located between these two types, modulate the magnitude of stimulation signals. The BONS possess the memory functions known as the synapse, which enables the regulation of signal strength between two neurons[4]. This synaptic strength changes adaptively in response to stimulation. Receptor neurons are capable of modulating their sensitivity to stimuli through the regulation of synaptic strength. Representative examples include sensitization and desensitization[5–7]. These two processes serve as a protective mechanism, enabling organisms to respond more efficiently to potential threats or alterations in their environment. Sensitization leads to a reduction in the threshold for stimulation while concurrently enhancing the magnitude of the response (Fig. 1b). On the other hand, desensitization refers to the process of attenuating background stimulus signals to improve the detection of new stimuli (Fig. 1c). Signals from receptor neurons are suitably modulated to facilitate perception as they transmit toward the cortex (Fig. 1d)[8–10]. Signals transmitted to the cortex are processed by an extensive network of cortical neurons and converted into olfactory perception (Fig. 1e).

Artificial olfactory systems (AOSs) that mimic the BONS have been developed for over 40 years[11–33]. However, in contrast to the versatility of the BONS, the functionalities of AOSs are still limited to basic gas identification tasks within limited settings. The limited capabilities of AOSs stand in stark contrast to the broad versatility of artificial vision

[1]Inter-university Semiconductor Research Center, Department of Electrical and Computer Engineering, Seoul National University, Seoul, Republic of Korea. [2]School of Transdisciplinary Innovations, Seoul National University, Seoul, Republic of Korea. [3]Department of Semiconductor Engineering, Gwangju Institute of Science and Technology (GIST), Gwangju, Republic of Korea. [4]Department of Semiconductor Convergence Engineering & Electrical and Computer Engineering, Sungkyunkwan University, Suwon, Republic of Korea. [5]Department of System Semiconductor Engineering, Sogang University, Seoul, Republic of Korea. e-mail: jhl@snu.ac.kr

https://doi.org/10.1038/s41467-026-76918-1

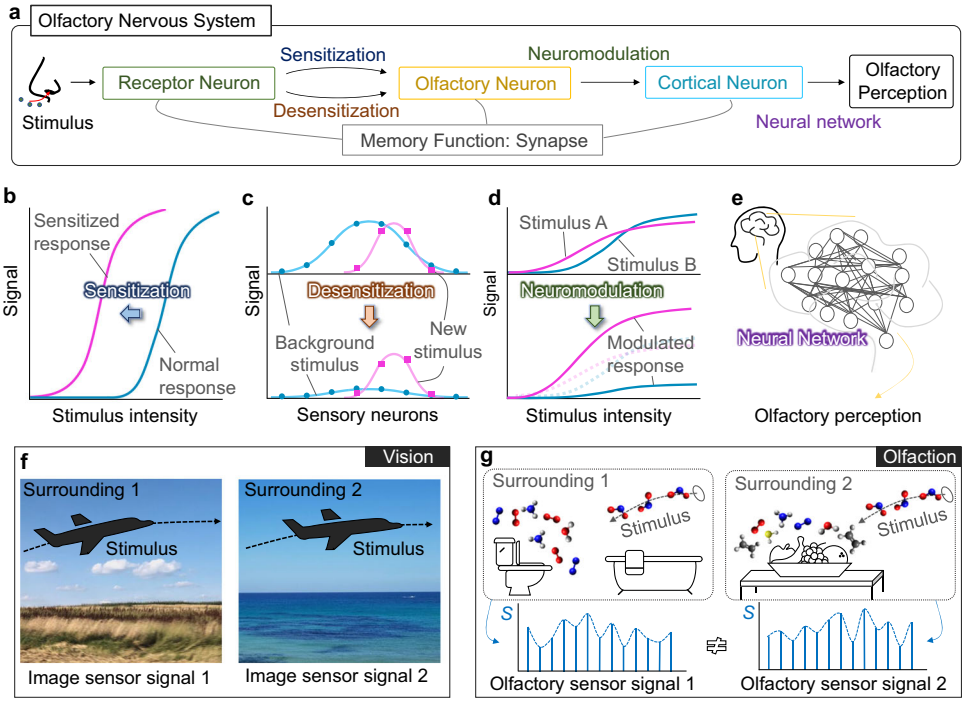


Fig. 1 | Olfactory nervous system with sensory adaptation functions. **a** Schematic diagram of the olfactory nervous system. Schematic images illustrating sensitization (**b**), desensitization (**c**), neuromodulation (**d**), and neural networks (**e**). **f** Schematic signals of image sensors from the visual stimulus (object) existing in two different surroundings. **g** Schematic olfactory sensor signals from the olfactory stimulus introduced in two different surroundings.

systems[34,35]. This disparity in performance arises because AOSs are significantly more affected by their surroundings compared to artificial vision systems. In artificial vision systems, the surrounding environment impacts the accuracy of object recognition; for example, by obscuring parts of the targeted visual stimulus (=object) within the image sensor signal. However, the intrinsic signal properties of the targeted visual stimulus rarely vary with its surroundings (Fig. 1f). On the other hand, in AOSs, the surrounding environment significantly affects the intrinsic signal properties of the olfactory sensors. Even with the introduction of the same target olfactory stimulus, sensor signals can vary significantly depending on surrounding conditions, making the unique pattern of the targeted stimulus less discernible (Fig. 1g). Therefore, for AOSs to become versatile and intelligent, they must train diverse signal patterns. Unfortunately, in the real world, there are countless combinations of ambient and target gases, each combination producing a different signal pattern. Therefore, even though the AOS learns numerous signal patterns in various environments, it may encounter unfamiliar patterns, which significantly reduces the accuracy of gas identification. Furthermore, if the AOS is configured with a limited number of olfactory sensors, gas identification becomes more difficult because different combinations of gases can result in nearly identical response signal patterns[12,13]. Therefore, to improve the performance of AOSs, a large number of sensors, extensive training data, a large neural network, and significant computational resources have been required.

Conventional AOSs adhere to the von Neumann architecture, where sensing, memory, and processing functions are executed in separate components (or chips)[12,23]. Therefore, they consume a lot of energy and necessitate extensive communication between components, leading to significant latency[12,14,31,32]. These limitations become more pronounced in intelligent and general-purpose AOSs, which rely heavily on data-driven learning. Therefore, to address these limitations, there is a move towards developing AOSs that enhance the integration of sensing, memory, and processing components both physically and functionally[20,23,36–38]. However, efficiently combining these three elements on the same substrate has seldom been achieved.

BONSs are capable of recognizing olfactory stimuli in diverse environments using sensory adaptation functions. They employ a strategy to enhance the perception accuracy of new olfactory stimuli by adapting the receptors to the surrounding environment through the desensitization process. However, AOSs have been developed with relatively little focus on emulating the sensory adaptation functions of the BONS. Previous efforts to imitate sensory adaptation functions have involved placing discrete memory components adjacent to olfactory sensors, with subsequent demonstrations that the characteristics of these memory elements can change in response to olfactory stimulation[37,39–42]. While these approaches enable the memory of stimulus history, they have difficulty replicating the efficiency of biological sensory adaptation functions.

Herein, we present an intelligent artificial olfactory nervous system (AONS) designed to mimic the functions of the BONS to achieve high versatility and efficiency. Similar to the structure of BONS, the AONS integrates artificial receptor neurons, artificial olfactory neurons, and artificial cortical neurons, all on a single substrate. The AONS functionally emulates the BONS based on a high level of integration of sensing, memory, and processing functions. The artificial receptor neurons can perform sensitization and desensitization functions, artificial olfactory neurons can modulate signals, and artificial cortical neurons can process the signal for olfactory perception. We demonstrate that the AONS can identify new stimuli (=gases) with high accuracy even in diverse surrounding environments by utilizing sensory adaptation functions.

Results and discussion

Overview of artificial olfactory nervous system

The AONS is fabricated using complementary metal–oxide–semiconductor (CMOS) compatible processes (see “Methods”). The AONS integrates eight artificial receptor neurons, eight artificial olfactory neurons, and six artificial cortical neurons on the same

https://doi.org/10.1038/s41467-026-76918-1

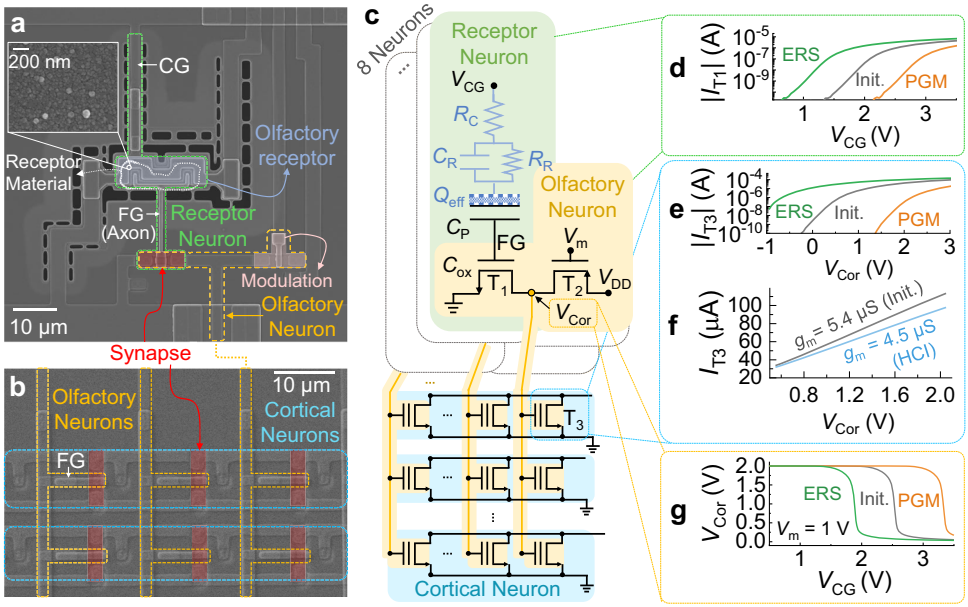


Fig. 2 | Artificial olfactory nervous system with memory functions. a Top SEM image of the AONS in a region where a receptor neuron and an olfactory neuron are integrated. The surface SEM image of SnO_2, the receptor material, is shown in the inset. **b** SEM image of AONS in a region where olfactory neurons and cortical neurons are integrated. **c** Schematic of the simplified equivalent circuit for the fabricated AONS. R_C, R_R, and C_R represent the contact resistance, receptor material resistance, and receptor material capacitance, respectively. C_P and C_{ox} denote the capacitances of the passivation layer and gate oxide, respectively. T_1, T_2, and T_3 represent the synapses of the receptor neuron, olfactory neuron, and cortical neuron, respectively. Programming and erasing characteristics of the synapses in receptor (**d**) and cortical (**e**) neurons via Fowler–Nordheim tunneling. **f** Changes in transconductance (g_m) of the synapse of cortical neurons using hot carrier injection. **g** Changes in V_{CG}–V_{Cor} curve characteristics owing to synaptic programming and erasing in receptor neurons.

substrate (Figs. 2a, b, and S1). This AONS combines sensing, memory, and computing functions efficiently in terms of both energy and space. The artificial receptor neuron (=gas sensor with memory function) is comprised of an olfactory receptor for detecting olfactory stimuli, an artificial axon responsible for signal transmission, and an artificial synapse (Figs. 1e, 2a, and S2). The olfactory receptor is composed of a control-gate (CG), a receptor material, and a part of a floating-gate (FG) that acts as an axon (Fig. S2). The voltage applied to the CG is transmitted to the FG, subsequently modulating the potential of the synaptic channel. The olfactory receptors detect olfactory stimuli utilizing the reactions between receptor materials and gases. The reaction leads to changes in the characteristics of the receptor material, including resistance (R), capacitance (C), and effective charge (Q_{eff}) (Fig. 2c). These changes alter the potential of the FG, functioning as a gate of the synapse, and change the conductance of the synapse. The detailed gas-sensing mechanism of receptor neurons will be discussed in the next section. A variety of materials can be used as receptor materials. Here, tin oxide (SnO_2) (Fig. S3), beneficial for its ability to detect a variety of gases and volatile organic compounds, is selected[43,44]. Beneath the receptor material, an ultra-low-power microheater is embedded to enhance gas-surface reactions[45]. Each of the eight receptor neurons is equipped with distinct microheaters, allowing each neuron to be operated at a different temperature (Fig. S4). As a result, they exhibit different responses to the same olfactory stimulus even with the same receptor material. This response pattern serves as a basis for gas identification, which will be covered in a later section. Note that because all eight receptor neurons employ the same sensing material, they can be fabricated in a single, uniform process flow without material-specific patterning steps. Using different sensing materials for all eight neurons would require multiple cycles of lithography, patterning, and deposition, increasing process complexity, lowering yield, and raising fabrication cost.

Olfactory neurons connect receptor neurons to cortical neurons (Fig. 2a–c). The *p*FET synapse of the olfactory neuron is connected in series to the *n*FET synapse of the receptor neuron (Fig. 2c). This complementary configuration allows signals from the receptor neurons to be effectively amplified and modulated before transmission to cortical neurons. The modulation voltage (V_m) applied to the gate of *p*FET can control the degree of modulation. The synaptic components of the cortical neuron are arranged in an AND type, and the word-lines (WLs) of the array are connected to the outputs of olfactory neurons. The voltage signal applied to the WLs is multiplied in parallel by the conductance values of synapses, and the results of the multiply-accumulate operation are output to the bit-lines of the array. The synapses of receptor and cortical neurons are *n*-type non-volatile memory devices with heavily doped polysilicon FG. These synaptic memory devices, programmable or erasable via Fowler–Nordheim (FN) tunneling and hot carrier injection (HCI) (Fig. 2d–f), determine the functional relationship between the signals outputted by the receptor neurons and those transmitted to the cortical neurons (Fig. 2g).

Sensory adaptation functions of artificial receptor neurons

The fabricated artificial olfactory receptor neurons can perform sensitization and desensitization functions. These sensory adaptation functions are achieved by exploiting the stimulus-sensing (=gas-sensing) mechanisms of the receptor neurons. Upon olfactory stimulation, the resistances and capacitances of receptor material change, and Q_{eff} is generated (Fig. 3a). The Q_{eff} changes the threshold voltage (V_{th}) of the receptor neuron. The negative Q_{eff} generated by oxidizing gas reactions increases the V_{th}, while the positive Q_{eff} produced by reducing gas reactions decreases the V_{th} (Fig. S5). Alterations in the resistances and capacitances change the coupling ratio characteristics between the CG and FG[46]. The reactions of receptor neurons to oxidizing and reducing gases slow down and speed up the transmission of V_{CG} to the FG and the synaptic channel, respectively. In other words, the reaction with oxidizing NO_2 gas increases the time constant (τ), whereas the reaction with reducing NH_3 gas decreases the τ (Figs. 3b and S6). An increase in τ from oxidizing gas exposure

https://doi.org/10.1038/s41467-026-76918-1

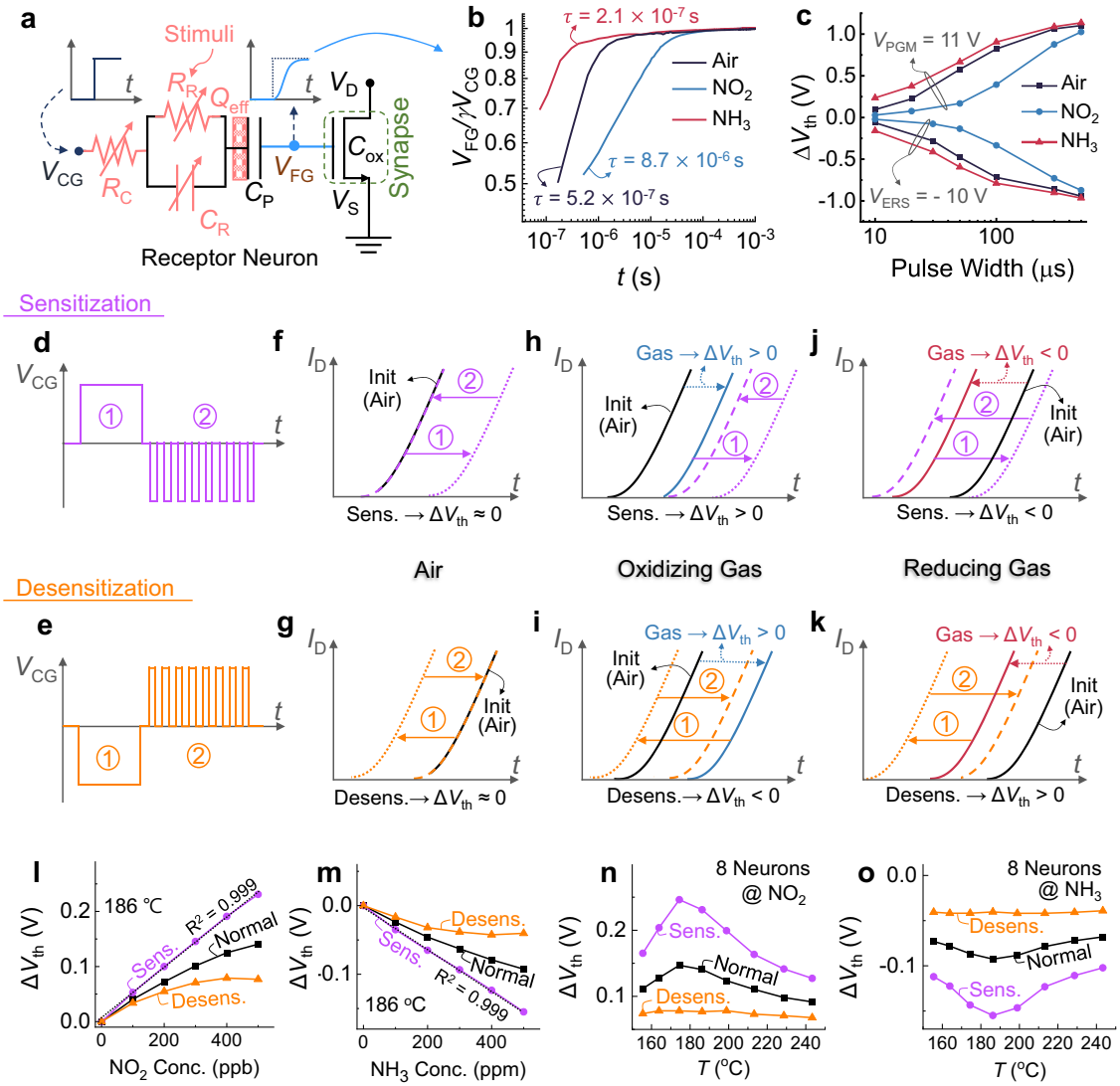


Fig. 3 | Sensory adaptation functions of artificial olfactory receptor neurons. **a** Schematic representation illustrating the changes in receptor neurons in response to stimulation. **b** Transient $V_{FG}/\gamma V_{CG}$ behavior of the olfactory receptor neuron after exposure to air, 250 ppm NH_3, and 500 ppb NO_2 gas atmospheres. The γ denotes V_{FG}/V_{CG} at a steady state. Time constants (τs) obtained by fitting the transient curve to the exponential decay curve are shown. **c** ΔV_{th} of receptor neurons owing to programming and erasing operations as a function of pulse width in air, 250 ppm NH_3, and 500 ppb NO_2 gas atmospheres. Schematic V_{CG} profiles to perform the sensitization (**d**) and desensitization (**e**) functions. Schematic transfer curves of receptor neurons before and after the sensitization (**f**, **h**, **j**) and desensitization (**g**, **i**, **k**) processes in air (**f**, **g**), oxidizing (**h**, **i**), and reducing (**j**, **k**) gas atmospheres. The solid arrows 1 and 2 in (**f**–**k**) denote ΔV_{th}s induced by a single long pulse and multiple short pulses, as shown in (**d**, **e**), respectively. The dotted arrows in (**h**–**k**) indicate ΔV_{th}s resulting from gas reactions. ΔV_{th}s of receptor neurons at various NO_2 (**l**) and NH_3 (**m**) gas concentrations before and after the sensitization and desensitization processes. Signal patterns of eight receptor neurons in response to 500 ppb NO_2 (**n**) and 250 ppm NH_3 (**o**) gases, before and after undergoing sensory adaptation processes. The normal cases of not using sensory adaptation processes are indicated by the lines with black squares (**l**–**o**).

effectively reduces the width and magnitude of programming/erasing pulses, decreasing $|\Delta V_{th}|$ due to program/erase. In contrast, a decrease in τ from reducing gas exposure effectively increases the width and magnitude of pulses, leading to a larger $|\Delta V_{th}|$ due to program/erase. In other words, the $|\Delta V_{th}|$ values from programming/erasing operations after exposure to oxidizing gases (e.g., NO_2) are smaller than those in the air (Fig. 3c). On the other hand, programming/erasing after exposure to reducing gases (e.g., NH_3) results in larger $|\Delta V_{th}|$ values compared to those in the air (Fig. 3c). The difference between the $|\Delta V_{th}|$ values in air and after gas reactions is significant with small pulse widths and becomes negligible when the pulse widths are sufficiently large (Fig. 3c).

The functions of sensitization and desensitization are implemented by exploiting the difference in programming and erasing characteristics owing to gas reactions. The schematic V_{CG} profiles to perform the sensitization and desensitization functions are illustrated in Fig. 3d, e, respectively. Both sensitization and desensitization profiles are composed of one long pulse and several short pulses. For sensitization, the long pulse is for programming, while in desensitization, it is for erasing. In the air, both sensitization and desensitization processes rarely change V_{th} because a single long pulse and multiple short pulses produce $|\Delta V_{th}|$s of approximately equal amounts but opposite signs (Fig. 3f, g). After reacting with oxidizing gases, the impact of short-width pulses on programming/erasing operations is reduced, making the long pulse dominant. As a result, neurons end up being programmed ($\Delta V_{th} > 0$) or erased ($\Delta V_{th} < 0$) following the sensitization (Fig. 3h) and desensitization (Fig. 3i) processes, respectively. On the other hand, reacting with reducing gases improves the impact of short-width pulses on programming/erasing operations. As a result, neurons are erased ($\Delta V_{th} < 0$) or programmed ($\Delta V_{th} > 0$) after the

processes of sensitization (Fig. 3j) and desensitization (Fig. 3k), respectively. Therefore, for both oxidizing and reducing gases, the sensitization and desensitization processes conducted after the gas reaction serve to enhance and reduce the sensing signal (=sum of ΔV_{th}s due to gas response and sensory adaptation processes), respectively (Table S1).

The effectiveness of the sensitization and desensitization processes depends on the intensity of the olfactory stimulus. The more gas molecules react with the receptor material, the larger the change in τ, and the greater the ΔV_{th} resulting from sensory adaptation processes (Fig. S7). Remarkably, this property allows the sensitization process to overcome the inherent limitations of olfactory stimuli detection mechanisms relying on surface–gas reactions. In surface–gas reactions, the sensing signal saturates as the gas concentration increases due to the finite number of surface sites (see normal cases in Fig. 3l, m)[47]. Therefore, linearity between gas concentration and sensing signal cannot be maintained in the high concentration range. Surprisingly, within the concentration range of primary interest for NO_2 and NH_3, the sensitization process was able to transform the previously saturated signal curves into highly linear ones (Figs. 3l, m, and S8). Additionally, sensitization can enhance the signal-to-noise ratio (SNR) of receptor neurons, with a more significant increase observed at higher gas concentrations (Fig. S10). However, since the sensitization process does not increase the amount of gas adsorbed onto the receptor neurons, the limit of detection (LoD) for the receptor neurons remains nearly unaffected by sensitization (Fig. S10).

The processes of sensitization and desensitization, respectively, make the sensing signal patterns for olfactory stimuli distinct and blurry. Note that the sensitization and desensitization processes can be performed simultaneously on multiple receptor neurons, thus influencing the signal patterns in a single process. Figure 3n, o display the signal patterns of eight receptor neurons to NO_2 and NH_3 gases before and after the sensory adaptation processes. The sensitization process amplifies the differences between the signals, whereas the desensitization process serves to diminish these differences. The desensitization process offers significant advantages for identifying new stimuli because it can eliminate surrounding environment-induced signal patterns. The details will be covered in subsequent sessions.

Applications of sensory adaptation processes

The BONS effectively employs sensitization and desensitization processes. The sensitization process enables rapid recognition and warning. The more often an organism is exposed to a specific smell, the more sensitized it becomes to that smell, enabling it to recognize that smell more quickly (Fig. 4a). Desensitization enables accurate and reliable perception. Organisms rapidly become accustomed to the background (=surrounding) smell through the desensitization process, ultimately enabling them to identify new olfactory stimuli more accurately (Fig. 4b). The fabricated AONS imitates these two essential sensory adaptation processes of the BONS, enabling both rapid recognition of familiar olfactory stimuli and precise identification of new stimuli through desensitization.

Artificial receptor neurons are capable of functioning in a sensitization mode, where they react sensitively to repeated stimulation, offering prompt alerts. This mode is well-suited for applications such as gas leak detection, as it is optimized for determining the presence of gases. Accurate gas concentration identification can be achieved using the desensitization mode. The sensitization process can be performed in two ways. One method is to activate the process when a sensing signal exceeds a predefined threshold (Fig. 4c), while the other is to activate the process at predetermined intervals (Fig. 4d). When the sensitization process is activated upon reaching a specific threshold, the ΔV_{th} resulting from sensory adaptation gradually increases with repeated stimulation. Receptor neurons become increasingly sensitive to that particular stimulus, thereby enhancing their ability to detect and alert to the presence of that stimulus more promptly. Therefore, even neurons that initially respond slowly to stimuli gradually become faster at recognizing them with repeated exposure (Fig. 4e). Irrespective of external background gases, this sensitization process allows the AONS to quickly detect potential threats, similar to BONS (Fig. S9). However, excessive sensitization may lead to an overly reduced threshold, which could result in false alarms. Therefore, it is important to consider setting a limit to prevent the threshold from dropping below a certain excessively low value.

Artificial receptor neurons can adapt to environmental changes through regular activation of sensitization processes. The longer a neuron is exposed to a stimulus and the stronger the stimulus (higher concentration), the better it adapts to that stimulus (Fig. 4d). As the stimulus disappears, ΔV_{th} due to adaptation slowly decreases. When a new stimulus appears, the receptor neuron adapts to that new stimulus. By consistently applying the same sensitization process, receptors can automatically adapt to varying environmental conditions. The rate of adaptation to the environment can be adjusted by changing the frequency of sensitization cycles. In practical applications, both strategies, performing sensitization at regular intervals and triggering it when a change in the signal is detected, can be used together. This approach accelerates signal changes due to gas adsorption or desorption, allowing the receptor neuron to respond or recover faster, which enhances the ability and reliability to detect gas changes in the environment.

Artificial receptor neurons have desensitization capabilities that allow them to quickly adapt to their surroundings and reliably detect new stimuli (=newly introduced gas). The desensitization process allows neurons to generate unique signal patterns for the newly introduced gas. In a clean background environment (dry air), signals from the eight receptor neurons can form a unique pattern for each gas (Fig. 4f). Moreover, the overall shape of these patterns can remain consistent despite changes in gas concentration (Fig. 4g). However, maintaining these patterns in real-world environments is impossible. In real environments, water vapor or residual gases are present in the surrounding environments, which interfere with the signal pattern of newly generated gases, making accurate identification difficult (Figs. 4h and S10a). Remarkably, the proposed desensitization process effectively reduces the influence of surrounding environments, making the signal pattern only affected by newly introduced gases (Figs. 4i and S10b). Even though NO_2 gas is introduced into four diverse surrounding environments (air, air with NO, NH_3, and H_2S residual gases), the output signal patterns of these settings can be similar by utilizing the desensitization process (Fig. 4j). Furthermore, the desensitization process is applicable under humid background conditions (Fig. S11). This desensitization process allows AONS to accurately identify gases regardless of previous gas exposure and diverse background environments.

The memories of stimulus-adapted receptor neurons can be reset (forgetting process, Fig. 4k). When AONS is relocated from a previous environment to a new one, the existing adapted memories of the receptor neurons may need to be forgotten. The memory of all receptor neurons can be easily reset with long erasing and programming pulses (Fig. 4l, m).

Sensory adaptation can also be applied to VOCs like acetone and ethanol. Through the sensitization process, the response of receptor neurons to acetone and ethanol gases becomes more linear with respect to gas concentration (Fig. S12a, b). Additionally, sensitization increases the SNR but does not lead to a significant change in the LoD (Fig. S12c, d). Furthermore, the response patterns of the eight receptor neurons can become more distinct with sensitization, while desensitization may blur these patterns (Fig. S13). Desensitization can also facilitate the formation of specific patterns for newly

https://doi.org/10.1038/s41467-026-76918-1

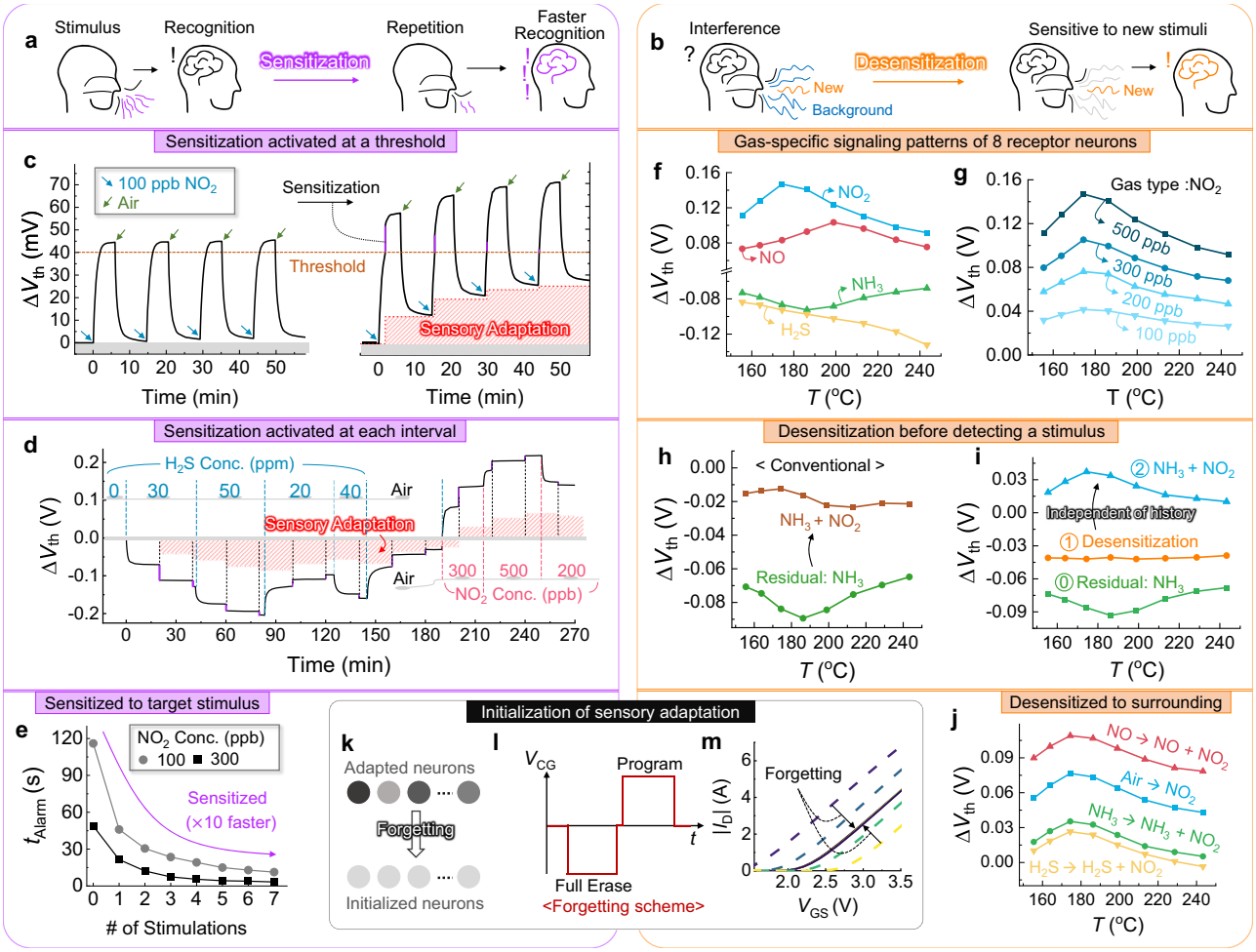


Fig. 4 | Applications of sensory adaptation processes. a Schematic images illustrating the rapid recognition of repetitive stimuli through the sensitization process. **b** Schematic images illustrating accurate detection of new stimuli through the desensitization process. **c** Dynamic ΔV_{th} behavior of neurons with (right figure) and without (left figure) sensitization in the environment where 100 ppb NO_2 gas is repeatedly injected. The threshold for activating the sensitization process is set to 40 mV, as an example. **d** Dynamic ΔV_{th} behavior of the neuron that periodically undergoes sensitization processes in a varying environment. In this example, the neuron is sequentially exposed to a changing environment, starting with H_2S gas, then to air, and finally to NO_2 gas. ΔV_{th}s resulting from sensitization are indicated by the hatched area. **e** Time (t_{alarm}) required to alert to a stimulus versus the number of repetitions of the stimulus. Sensitization processes are performed for each repeated stimulation. The t_{alarm} is defined as the time required for the sensing signal to reach a ΔV_{th} of 40 mV. **f** Signal patterns of eight receptor neurons for 500 ppb NO_2, 500 ppb NO, 250 ppm NH_3, and 50 ppm H_2S gases. **g** Signal patterns of eight receptor neurons in various concentrations of NO_2 gas atmosphere. Signal patterns of eight receptor neurons when 200 ppb NO_2 is injected after the reaction with 250 ppm NH_3 gas, with (**i**) and without (**h**) the desensitization process. **j** Signal patterns of eight receptor neurons in response to 200 ppb NO_2 introduced into various surroundings (air, air + 200 ppb NO, +250 ppm NH_3, and +50 ppm H_2S gases) when using the desensitization processes. **k** Schematic image of the forgetting process that resets memories in adapted neurons. **l** Schematic V_{CG} profile scheme of the forgetting process. **m** Transfer curves of variously adapted neurons before and after performing the forgetting processes.

introduced gases, irrespective of the types of residual gases (Fig. S13).

Signal modulation capabilities of artificial olfactory neurons

Olfactory neurons modulate signals from receptor neurons and transmit them to cortical neurons (Fig. 5a). The *p*FET synapse of the olfactory neuron is connected in series with the *n*FET synapse of the receptor neuron (Fig. 5b). The voltage (V_m) applied to the gate of the *p*FET serves as a modulation knob, adjusting how the signal (ΔV_{th}) of the receptor neuron is converted into the signal (V_{Cor}) transmitted to the cortical neurons. The V_m determines the shape of the V_{CG}–V_{Cor} curve (Fig. 5c), and the slope of this curve directly affects the signal amplification gain (A_V) (Fig. 5d). Receptor neurons respond to reducing and oxidizing gases, producing negative and positive ΔV_{th} signals, respectively (Fig. 5e). These negative and positive ΔV_{th}s cause the V_{CG}–V_{Cor} curve to shift in negative and positive directions, respectively, and decrease and increase the V_{Cor} (Fig. 5f).

By adjusting V_m and V_{CG}, olfactory neurons can selectively regulate the degree of signal amplification for specific types of stimulation. Given that oxidizing and reducing gases produce ΔV_{th} with opposing signs, selective signal amplification can be achieved by adjusting the V_m setting while keeping V_{CG} constant. For example, with V_{CG} fixed at 2.34 V and V_m set to 1.2 V, the $\Delta V_{Cor}/\Delta V_{th}$ is large for oxidizing gases but small for reducing gases (Fig. 5g). Conversely, adjusting V_m to 1.07 V results in a large $\Delta V_{Cor}/\Delta V_{th}$ for reducing gases and a small $\Delta V_{Cor}/\Delta V_{th}$ for oxidizing gases (Fig. 5g). Adjusting V_m can selectively increase the sensitivity of the ΔV_{Cor} to either oxidizing or reducing gases (Fig. 5h–j). Moreover, by modulating V_m, the V_{Cor} signal pattern can be manipulated to be distinct for oxidizing or reducing gases (Fig. S14).

By adjusting V_{CG} while holding V_m constant, the olfactory neurons can shift the baseline of the V_{Cor} signal. The ΔV_{th} is comprises a background-induced reference component V_R and target gas-induced term $\Delta(\Delta V_{th})$ (=$\Delta V_{th} - V_R$) (Figs. 5k and S15), and both V_R and $\Delta(\Delta V_{th})$

https://doi.org/10.1038/s41467-026-76918-1

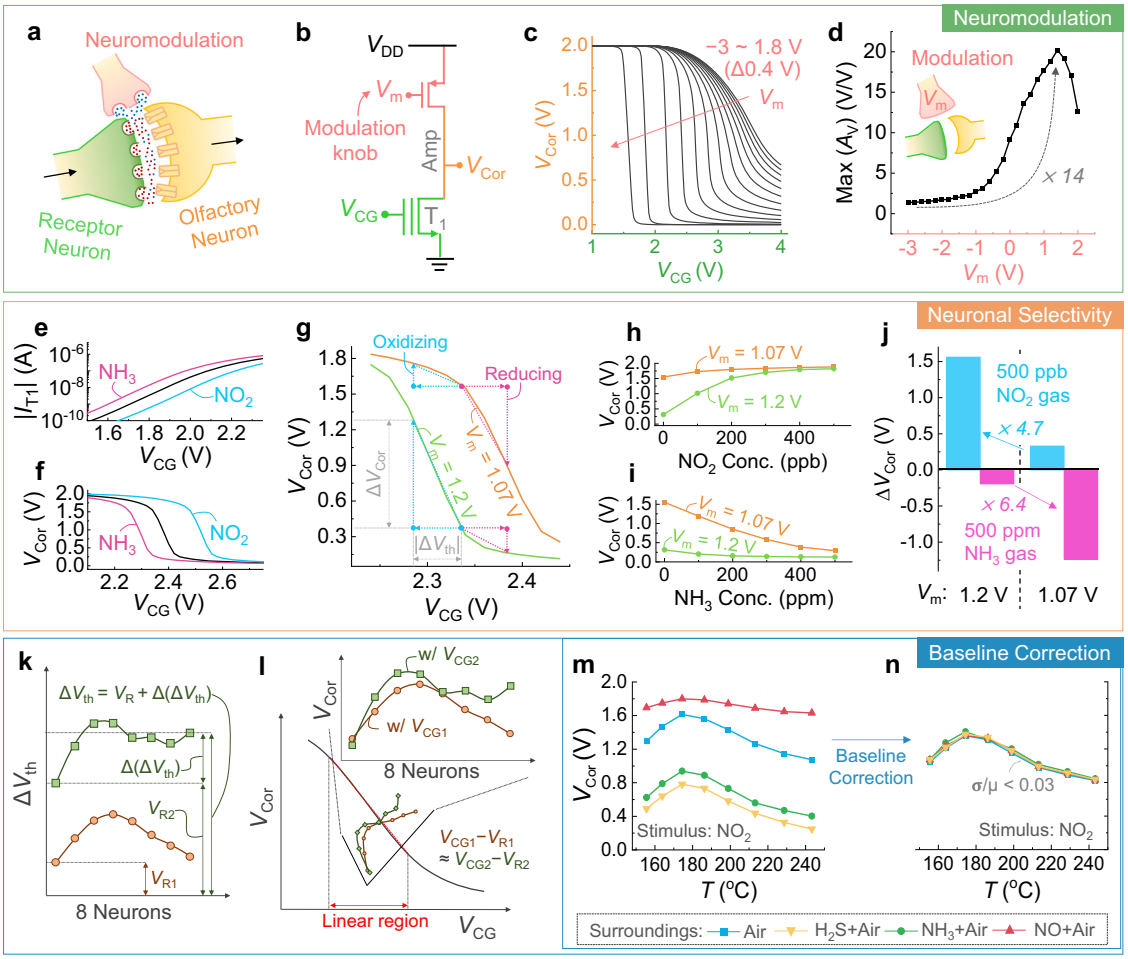


Fig. 5 | Signal modulation capabilities of artificial olfactory neurons. **a** Schematic illustration depicting the modulation of sensing signals by olfactory neurons. **b** Simplified equivalent circuit for the section connecting the *n*FET synapse of the receptor neuron to the *p*FET synapse of the olfactory neuron. **c** V_{CG}–V_{Cor} curves of olfactory neurons under various V_m conditions at a V_{DD} of 2 V. **d** Signal amplification (gain: A_V) of the sensing signal as a function of the V_m. **e** Transfer curve of receptor neurons before and after response to 500 ppb NO_2 and 500 ppm NH_3 gases at a V_{DS} of 1 V. **f** V_{CG}–V_{Cor} curves before and after the 500 ppb NO_2 and 500 ppm NH_3 gas reactions at a V_m of 1 V. **g** V_{CG}–V_{Cor} curves at V_m of 1.2 and 1.07 V in dry air. ΔV_{Cor} at various concentrations of NO_2 (**h**) and NH_3 (**i**) gases at V_ms of 1.2 and 1.07 at V_{CG} of 2.34 V. **j** ΔV_{Cor} for 500 ppb NO_2 and 500 ppm NH_3 gases at V_m of 1.2 and 1.07 V at V_{CG} of 2.34 V. **k** V_{Cor} pattern for 200 ppb NO_2 gas at V_{CG}s of 2.32 and 2.34 V. **l** V_{Cor} signal patterns resulting from the introduction of 200 ppb NO_2 gas into four different surrounding environments (Air, Air + 200 ppb NO, 250 ppm NH_3, and 50 ppm H_2S residual gases), utilizing the desensitization process. **m**-**n** V_{Cor} signal patterns when NO_2 gas is introduced into four surrounding environments, employing desensitization alone (**m**) and combined baseline correction and desensitization (**n**).

can influence the V_{Cor} pattern. By tuning V_{CG}, the effective contribution of V_R can be meaningless (driven to a common), negligible baseline, so that the V_{Cor} readout is dominated by the target-dependent $\Delta(\Delta V_{th})$. As illustrated in Fig. 5l, choosing an appropriate V_{CG} converts two ΔV_{th} patterns with different baseline into V_{Cor} signals with a similar baseline. Additionally, if V_{CG} is selected so that the mapping from $\Delta(\Delta V_{th})$ to ΔV_{Cor} operates in a linear regime, baseline correction and amplification occur simultaneously without distorting the receptor pattern. In this case, all ΔV_{Cor} values are determined by multiplying the same gain (=$\Delta V_{Cor}/\Delta V_{th}$), ensuring that the V_{Cor} pattern faithfully preserves the ΔV_{th} pattern.

Figure 5m, n show the V_{Cor} signal patterns resulting from introducing NO_2 gas into four distinct surrounding environments without and with baseline correction, respectively. The V_{Cor} patterns are generated by transforming the ΔV_{th} patterns. As shown in Fig. 4j, because desensitization was applied at the receptor-neuron level, the ΔV_{th} patterns have similar shapes but different baselines. Consequently, when these baseline-shifted ΔV_{th} patterns are converted to V_{Cor} using the same readout condition, the resulting V_{Cor} waveforms exhibit similar shapes yet markedly different baselines, as in Fig. 5m. Moreover, in the environment containing residual NO, the conversion from ΔV_{th} to V_{Cor} occurs in the nonlinear region of the V_{CG}–V_{Cor} characteristic, causing pattern distortion (Fig. 5m). In contrast, applying the baseline-correction method, selecting V_{CG} while accounting for the V_R appropriate to each ΔV_{th} pattern, aligns the baselines of the resulting V_{Cor} signals and prevents distorted amplification, as shown in Fig. 5n. Thus, the similar ΔV_{th} patterns obtained through desensitization can be reliably converted into similarly shaped V_{Cor} patterns.

Cortical neurons and gas identification

Cortical neurons process signals from olfactory neurons for olfactory perception (Fig. 6a). The fabricated cortical neurons process V_{Cor} signals in parallel, converting them into bit-line currents (I_{BL}s) of the synapse array (Fig. 6b). The AND-type synapse array supports selective programming and vector-matrix multiplication (VMM) operations. The threshold voltage of each synapse can be fine-tuned using HCI and FN tunneling. The I_{BL}, representing the sum of synapse cell currents, closely matches the summation of currents from each synapse cell (I_{syn}s) (Fig. 6c), ensuring accurate and reliable VMM operation. Specifically,

https://doi.org/10.1038/s41467-026-76918-1

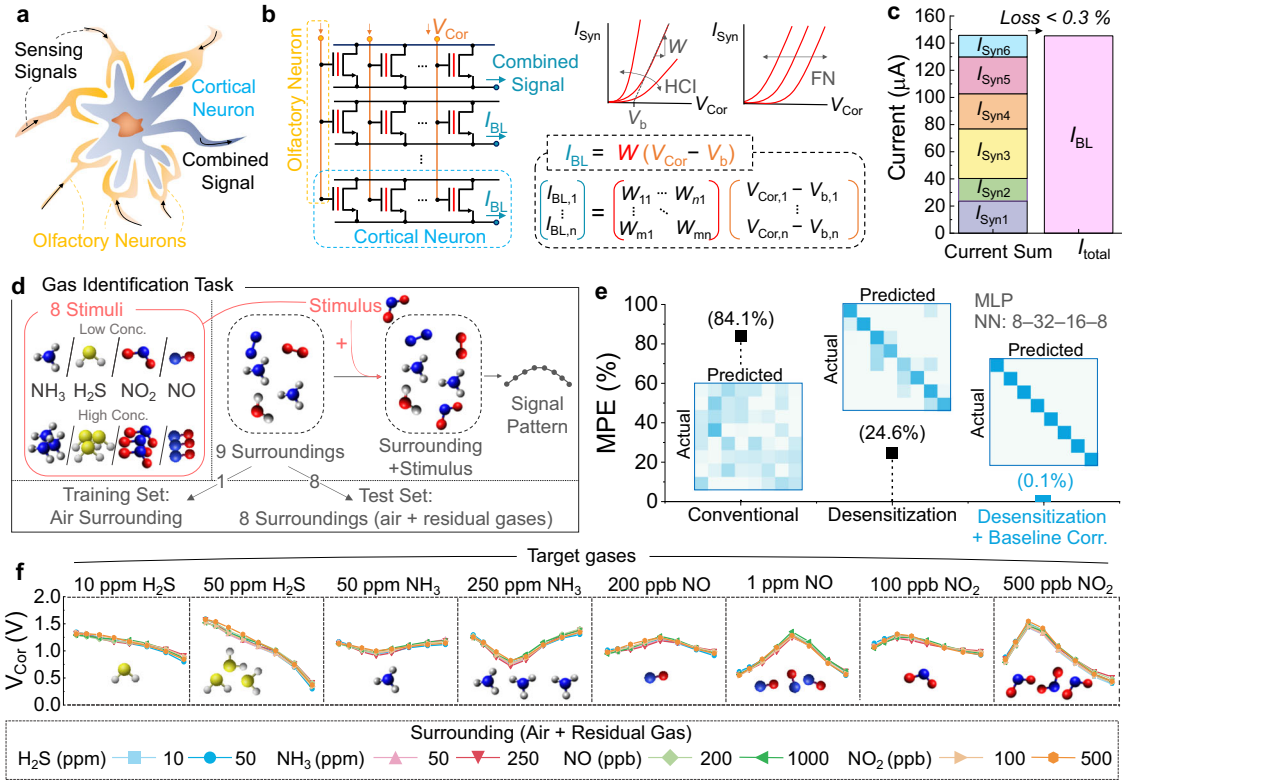


Fig. 6 | Artificial cortical neurons and gas identification. a Schematic illustration depicting the transmission of sensing signals and signal processing in cortical neurons. **b** Schematic image illustrating the processing of sensing signals in artificial cortical neurons. The schematic diagram on the right illustrates that the conductance weight (W) and voltage bias (V_b) of each cell can be adjusted via hot carrier injection (HCI) and Fowler–Nordheim (FN) tunneling. **c** Comparison of total array current ($I_{BL} = I_{total}$) and summed cell currents (I_{syn}s). **d** Schematic image of the gas identification task. **e** Mean percentage error (MPE) and confusion matrix for the gas identification task under three cases: conventional, using the desensitization process, and using a combination of desensitization with baseline correction processes. **f** V_{Cor} patterns for a total of 64 combinations involving eight surroundings (air + residual gases) and eight target gases when using the desensitization and baseline correction processes.

the conductance of the memory cells used as synapses encodes the weights, and the V_{Cor} signals are applied as gate voltages (inputs) to those synaptic cells. The applied V_{Cor} inputs are multiplied in parallel by the synaptic conductances, and the resulting products are summed on the bit line to form the bit-line current. This implements a conventional compute-in-memory (analog multiply–accumulate) operation. Note that, in this study, we designed and fabricated only a portion of the artificial cortex, focusing on demonstrating the ability of artificial cortical neurons to process signals of artificial olfactory neurons. Our AONS is fully compatible with and complements existing studies on hardware-based artificial cortexes[48–51]. Therefore, we believe our AONS has significant potential for further development.

Here, we demonstrate that combining desensitization with baseline correction enables reliable gas identification in realistic environments. In realistic environments, the AONS may encounter extensive combinations of backgrounds and target gases. However, it is impractical to train the system across all possible environments. Thus, we validated the effectiveness of this sensory adaptation technique by intentionally constructing a highly challenging environment, where the presence of background gases at levels similar to the target gas severely hinders the learning process. By employing a two-step pipeline, desensitization followed by baseline correction, responses in new environments are made to closely resemble those measured in air, thereby improving reliability and enabling models trained primarily in air to generalize. Accordingly, the AONS was trained in air and then evaluated across eight distinct surroundings with severe residual-gas interference (Fig. 6d), using eight target conditions (two concentrations each of NO_2, NO, NH_3, and H_2S). Figure 6e illustrates the mean percentage error (MPE) and confusion matrix of three cases: normal (=conventional), employing the desensitization process, and employing both the desensitization and baseline correction processes. The MPE in the conventional case is very high (84.1%), but when desensitization and baseline correction processes are applied together, the MPE drops to 0.1%. This performance enhancement stems from improved data quality rather than the specific algorithm used. Indeed, numerous existing machine learning studies assert that high uniformity in both training and inference data is a critical prerequisite for improving overall system performance[52–54]. This improvement reflects the near-invariance of V_{Cor} to the surroundings (Fig. 5f) and the resulting consistency of target-gas patterns, in sharp contrast to the variability observed without processing (Fig. S16).

To verify its practical applicability, we exposed the AONS to the gases emitted from spoiling chicken tenderloins and applied the proposed adaptation method (Fig. S17). We then compared the sensor signals obtained from the actual meat spoilage with those acquired in an artificially mixed NH_3 and H_2S gas environment, confirming a remarkable consistency between the two. This demonstrates that the proposed AONS can successfully identify the distinct gas patterns associated with meat decay, namely the initial emission of NH_3 followed by the release of H_2S during severe putrefaction[55]. Ultimately, these results prove that our proposed method transcends simple gas identification and can be successfully implemented in practical, real-world applications driven by complex gas recognition.

Table S2 provides benchmarks for state-of-the-art artificial olfactory systems[22,29,33,42]. Whereas most prior systems require environment-specific retraining, the proposed AONS operates across

diverse backgrounds without extra training owing to its sensory-adaptation pipeline. This reduces both network size and training-data requirements, yielding benefits in energy consumption. By mimicking the sensory-adaptation function of the biological olfactory neural system, the proposed AONS offers a practical route to reliable and scalable artificial olfaction in complex settings.

This work reported an intelligent artificial olfactory neural system (AONS) endowed with biologically inspired sensory adaptation. Biological olfaction performs both sensitization and desensitization; while the proposed AONS cannot execute them simultaneously, it is configured in either mode to reproduce the essential functions. In sensitization, repeated exposure to a known target heightened the effective sensitivity of the ANOS to that target, enabling faster and more reliable confirmation of its presence. In desensitization, the ANOS adapted to the ambient environment by suppressing response components shared with the background, thereby isolating a clear, target-specific pattern when a previously unseen gas appeared. Accordingly, mode selection can be aligned with the objective: sensitization for repeated verification of a particular gas, and desensitization for identification of unknown analytes amid diverse backgrounds.

The AONS comprised receptor neurons, olfactory neurons, and cortical neurons. Receptor neurons integrated sensing and memory and operated in the two task-dependent modes described above. Olfactory neurons amplified and modulated sensing signals, enabling neuronal selectivity and baseline correction of response patterns. Cortical neurons employed a synapse array to process signals from the olfactory layer toward olfactory perception. Despite being trained under limited settings, the AONS accurately identified eight distinct stimuli across eight different environments by effectively leveraging desensitization and baseline correction. Although we demonstrated the identification capability for only eight gas species, our adaptation method can consistently capture the unique patterns of various novel gases regardless of background interference. Thus, provided these patterns are pre-labeled and learned, the proposed AONS possesses a high potential to successfully identify a broad spectrum of new gases beyond those demonstrated here. Furthermore, we detected the gases emitted during the spoilage of chicken tenderloins using the proposed AONS and obtained clearly distinct response patterns. This successfully demonstrates its broad applicability to various real-world applications. These results indicate a promising path toward intelligent, versatile artificial olfactory systems designed for operation in complex application environments.

Methods

Fabrication

The AONS was fabricated using standard complementary CMOS techniques on a 6-inch, *p*-type, bulk Si wafer with a (100) orientation. A 10-nm-thick sacrificial oxide layer was deposited via low-pressure chemical vapor deposition (LPCVD) to protect the substrate during *n*-well implantation for *p*-channel devices (P^+, 120 keV, 3×10^{12} cm^{-2}). After the drive-in process (11 h, 1100 °C), a 10-nm-thick SiO_2 (buffer oxide) layer and a 140-nm-thick Si_3N_4 layer were sequentially formed. These layers were patterned to define the active areas. Then a field implantation (B^+, 40 keV, 1.6×10^{13} cm^{-2}) was carried out. The local oxidation of silicon (LOCOS) technique was employed for the electrical isolation of adjacent devices, involving thermal oxidation to form a 450-nm-thick field oxide layer. After removing the buffer oxide layer and the nitride layer, a sacrificial oxide layer was grown through a thermal oxidation process. The ion implantation for threshold voltage (V_{th}) adjustment was conducted, and then the sacrificial oxide layer was removed. A 10-nm-thick gate oxide was thermally grown. A 300-nm-thick in situ n^+-doped poly-Si layer was deposited by LPCVD. Source and drain implantation for *n*-channel (As^+, 40 keV, 2×10^{15} cm^{-2}) and *p*-channel (BF_2^+, 25 keV, 2×10^{15} cm^{-2}) was performed. The SiO_2 (9 nm)/Si_3N_4 (18 nm)/SiO_2 (9 nm) passivation layer was deposited following 1050 °C rapid thermal processing for 5 s. After the definition of contact holes, metal layers of Ti (20 nm)/TiN (30 nm)/Al (70 nm)/TiN (20 nm) were sequentially deposited and patterned. A hydrogen alloying process was carried out at 400 °C for 10 min. To improve thermal efficiency, an air gap was formed underneath the heater. Finally, the 14-nm-thick SnO_2 sensing layer was deposited and patterned.

Measurement of olfactory stimulus (=gas) response characteristics

The olfactory stimulation-response (gas-sensing) characteristics of the AONS were measured using a homemade probe station equipped with gas injection and ejection capabilities, along with a semiconductor parameter analyzer (B1500A, Agilent). After adjusting the humidity and gas concentration in the mixing chamber, gases were injected into the probe station. The receptor neurons operated between 155 and 245 °C. Temperatures below 155 °C did not yield distinctive patterns (Fig. S18), whereas substantially higher temperatures can compromise heater reliability. The ΔV_{th} in response to gas exposure by the receptor neuron was determined by comparing the changes in V_{th} of the transfer curves before and after gas interaction. The V_{th} of the transfer curve was calculated using the constant current method. The transient $V_{FG}/\gamma V_{CG}$ behavior of the olfactory receptor neuron was obtained through the transient current behavior of synapses (Fig. S6). The time constant (τ) of the transient curve was obtained by fitting the curve to an exponential decay curve. During the gas reaction, the temperature of the receptor material was regulated by an embedded microheater. Energy consumption was minimized by applying pulse-type voltage to this microheater (Fig. S4). The concentrations of the gases used in the experiments (NO_2, NO, NH_3, H_2S, and acetone) were set with reference to the standards of the United States Environmental Protection Agency (EPA) and the Occupational Safety and Health Administration (OSHA) and were selected to reflect the differing hazard levels of each gas. For the chicken tenderloin spoilage detection setup, dry air was injected into the container holding the food sample at a flow rate of 200 mL min^{-1}, and the gases emitted from the food were introduced into the main chamber containing the AONS. All other measurement conditions were identical to those used for the target gas characterization

Sensory adaptation processes

The V_{CG} profile for the sensitization process consists of one pulse of 500 µs width with $V_{PGM} = 11$ V and eight pulses of 42 µs width with $V_{ERS} = -10$ V. On the other hand, the V_{CG} profile for the desensitization process consists of one pulse of 500 µs width with $V_{ERS} = -10$ V and eight pulses of 38 µs width with $V_{PGM} = 11$ V. The degree of sensory adaptation can be further enhanced by repeating these profiles several times. Desensitization was achieved by iteratively applying the desensitization profile until the sensor response patterns became effectively patternless.

Additionally, various sensitization and desensitization profiles can be formed by adjusting the values of V_{PGM} and V_{ERS} and their pulse widths. Increasing the pulse widths and voltage values within a block can enhance the degree of sensory adaptation. For instance, a block consisting of one 500 µs pulse with $V_{PGM} = 11$ V and eight 42 µs pulses with $V_{ERS} = -10$ V will result in a higher degree of sensory adaptation compared to a block consisting of a 300 µs pulse with $V_{PGM} = 10$ V and five 40 µs pulses with $V_{ERS} = -9.5$ V.

Signal-to-noise ratio (SNR) and limit of detection

To examine the SNRs and LoDs of the receptor neurons, low-frequency noise and power spectral density were measured using a current amplifier (SR 570) and a dynamic signal analyzer (35670A). The LoD was evaluated using the method outlined in the IUPAC regulations[56]. The LoD is defined as the concentration at which the SNR equals 3.

Since the relationship between SNR and gas concentration follows a power-law dependence, the LoD was derived from the estimated slope of the log-log plot of SNR versus gas concentration (Figs. S10 and S12).

Forgetting processes

The receptor neurons, each having adapted to different stimuli and possessing distinct memories, can be reset. The process of forgetting these neurons is very similar to resetting memory devices. First, a sufficiently long erase pulse is applied to fully erase the receptor neurons. Then, a sufficiently long program pulse is applied to reset the memory of the receptor neurons to their initial state. It is crucial to use long enough pulses during both the erase and program steps to ensure that all receptor neurons, regardless of their previous environmental exposure, return to the same initial memory state. Note that when the program and erase pulses are short, the receptor neurons are programmed and erased to varying degrees depending on whether they were exposed to oxidative or reductive gases. However, when the pulse duration is sufficiently long, all neurons are programmed and erased to a similar extent.

Gas identification

The goal of gas identification is to distinguish between eight types of gas stimuli regardless of the surroundings, even though AONS was trained in a limited setting. The eight V_{Cor} signal values generated by the AONS in response to eight different gas stimuli that occurred in an air surrounding (total 8×1 stimulus-surrounding combinations) and eight surroundings with residual gases (total 8×8 stimulus-surrounding combinations) were utilized as training and test data, respectively. The eight gas stimuli are 100 and 500 ppb NO_2, 200 and 1000 ppb NO, 50 and 250 ppm NH_3, and 10 and 50 ppm H_2S. The eight different surroundings with residual gases are air mixed with 100 and 500 ppb NO_2, 200 and 1000 ppb NO, 50 and 250 ppm NH_3, and 10 and 50 ppm H_2S. Note that these surrounding conditions are severe cases because they contain residual gases equal to gas stimulation. The obtained training and test data were 1000 times augmented using a Gaussian distribution while maintaining a coefficient of variation of 0.1 (Note S1). While support vector machine and gradient boosting showed MPE trends similar to MLP (Note S2 and Fig. S19), this study centered on an MLP-based classifier owing to its suitability for hardware implementation. The multilayer perceptron classifier (hidden layer size: 32–16) was trained with an Adam optimizer, ReLU activation function, a total of 200 epochs, and early stopping when the model does not improve for 40 epochs.

Data availability

The data are available from the corresponding author upon request

References

1. Shepherd, G. M. Discrimination of molecular signals by the olfactory receptor neuron. *Neuron* **13**, 771–790 (1994).
2. Zatorre, R. J., Jones-Gotman, M., Evans, A. C. & Meyer, E. Functional localization and lateralization of human olfactory cortex. *Nature* **360**, 339–340 (1992).
3. Bhandawat, V., Reisert, J. & Yau, K. W. Cell signaling: elementary response of olfactory receptor neurons to odorants. *Science* **308**, 1931–1934 (2005).
4. Choquet, D. & Triller, A. The dynamic synapse. *Neuron* **80**, 691–703 (2013).
5. Guo, H. & Smith, D. P. Odorant receptor desensitization in insects. *J. Exp. Neurosci.* **11**, 1179069517748600 (2017).
6. Yee, K. K. & Wysocki, C. J. Odorant exposure increases olfactory sensitivity: olfactory epithelium is implicated. *Physiol. Behav.* **72**, 705–711 (2001).
7. Dewan, A. et al. Single olfactory receptors set odor detection thresholds. *Nat. Commun.* **9**, 2887 (2018).
8. Vaccari, F. E., Diomedi, S., Filippini, M., Hadjidimitrakis, K. & Fattori, P. New insights on single-neuron selectivity in the era of population-level approaches. *Front. Integr. Neurosci.* **16**, 929052 (2022).
9. Womelsdorf, T. et al. Orientation selectivity and noise correlation in awake monkey area V1 are modulated by the gamma cycle. *Proc. Natl. Acad. Sci. USA* **109**, 4302–4307 (2012).
10. Luo, T. Z. & Maunsell, J. H. R. Neuronal modulations in visual cortex are associated with only one of multiple components of attention. *Neuron* **86**, 1182–1188 (2015).
11. Persaud, K. & Dodd, G. Analysis of discrimination mechanisms in the mammalian olfactory system using a model nose. *Nature* **299**, 352–355 (1982).
12. Röck, F., Barsan, N. & Weimar, U. Electronic nose: current status and future trends. *Chem. Rev.* **108**, 705–725 (2008).
13. Park, S. Y. et al. Chemoresistive materials for electronic nose: progress, perspectives, and challenges. *InfoMat* **1**, 289–316 (2019).
14. Cole, M., Covington, J. A. & Gardner, J. W. Combined electronic nose and tongue for a flavour sensing system. *Sens. Actuators B Chem.* **156**, 832–839 (2011).
15. Covington, J. A., Marco, S., Persaud, K. C., Schiffman, S. S. & Nagle, H. T. Artificial olfaction in the 21st century. *IEEE Sens. J.* **21**, 12969–12990 (2021).
16. Kim, C. et al. Artificial olfactory sensor technology that mimics the olfactory mechanism: a comprehensive review. *Biomater. Res.* **26**, 40 (2022).
17. Guo, L., Yang, Z. & Dou, X. Artificial olfactory system for trace identification of explosive vapors realized by optoelectronic Schottky sensing. *Adv. Mater.* **29**, 1604528 (2017).
18. Jung, G. et al. Energy efficient artificial olfactory system with integrated sensing and computing capabilities for food spoilage detection. *Adv. Sci.* **10**, 2302506 (2023).
19. Wang, G., Li, Y., Cai, Z. & Dou, X. A colorimetric artificial olfactory system for airborne improvised explosive identification. *Adv. Mater.* **32**, e1907043 (2020).
20. Han, J. K. et al. Artificial olfactory neuron for an in-sensor neuromorphic nose. *Adv. Sci.* **9**, e2106017 (2022).
21. Kwon, D. et al. Efficient fusion of spiking neural networks and FET-type gas sensors for a fast and reliable artificial olfactory system. *Sens. Actuators B Chem.* **345**, 130419 (2021).
22. Chun, S. Y. et al. An artificial olfactory system based on a chemimemristive device. *Adv. Mater.* **35**, e2302219 (2023).
23. Liu, L., Zhang, Y. & Yan, Y. Four levels of in-sensor computing in bionic olfaction: from discrete components to multi-modal integrations. *Nanoscale Horiz.* **8**, 1301–1312 (2023).
24. Wan, C. et al. Artificial sensory memory. *Adv. Mater.* **32**, 1902434 (2020).
25. Qian, C. et al. Oxygen-detecting synaptic device for realization of artificial autonomic nervous system for maintaining oxygen homeostasis. *Adv. Mater.* **32**, 2002653 (2020).
26. Chouhdry, H. H., Lee, D. H., Bag, A. & Lee, N. E. A flexible artificial chemosensory neuronal synapse based on chemoreceptive ionogel-gated electrochemical transistor. *Nat. Commun.* **14**, 821 (2023).
27. Lee, S.-W. et al. An artificial olfactory sensory neuron for selective gas detection with in-sensor computing. *Device* **1**, 100063 (2023).
28. Lee, S., Kim, S., Nam, G. B., Eom, T. H. & Jang, H. W. Chemoresistive gas sensors for food quality monitoring. *J. Semicond. Technol. Sci.* **22**, 244–258 (2022).
29. Wang, C. et al. Biomimetic olfactory chips based on large-scale monolithically integrated nanotube sensor arrays. *Nat. Electron.* **7**, 842 (2024).
30. Kang, H. et al. Multiarray nanopattern electronic nose (E-Nose) by high-resolution top-down nanolithography. *Adv. Funct. Mater.* **30**, 2002486 (2020).

31. Gardner, J. W., Guha, P. K., Udrea, F. & Covington, J. A. CMOS interfacing for integrated gas sensors: a review. *IEEE Sens. J.* **10**, 1833–1848 (2010).
32. Hatfield, J. V., Covington, J. A. & Gardner, J. W. GasFETs incorporating conducting polymers as gate materials. *Sens. Actuators B Chem.* **65**, 253–256 (2000).
33. Sung, S. H. et al. Data-centric artificial olfactory system based on the eigengraph. *Nat. Commun.* **15**, 1211 (2024).
34. Lomonaco, V. et al. CVPR 2020 continual learning in computer vision competition: approaches, results, current challenges and future directions. *Artif. Intell.* **303**, 103635 (2022).
35. Mennel, L. et al. Ultrafast machine vision with 2D material neural network image sensors. *Nature* **579**, 62–66 (2020).
36. Zhou, F. & Chai, Y. Near-sensor and in-sensor computing. *Nat. Electron.* **3**, 664–671 (2020).
37. Wang, T. et al. A bio-inspired neuromorphic sensory system. *Adv. Intell. Syst.* **4**, 2200047 (2022).
38. Li, Z. et al. A miniature electronic nose for breath analysis. In *Proc. Technical Digest - International Electron Devices Meeting, IEDM* Vols 2021 (IEEE, 2021).
39. Wang, L., Li, W., Wan, L. & Wen, D. An artificial olfactory system based on a memristor can simulate organ injury and functions in air purification. *ACS Sens.* **8**, 4810–4817 (2023).
40. Ban, C. et al. An artificial olfactory memory system for monitoring and recording of volatile organic compounds. *Adv. Mater. Technol.* **6**, 2100366 (2021).
41. Shulaker, M. M. et al. Three-dimensional integration of nanotechnologies for computing and data storage on a single chip. *Nature* **547**, 74–78 (2017).
42. Gao, Z. et al. An artificial olfactory system with sensing, memory and self-protection capabilities. *Nano Energy* **86**, 106078 (2021).
43. Masuda, Y. Recent advances in SnO_2 nanostructure based gas sensors. *Sens. Actuators B Chem.* **364**, 131876 (2022).
44. Das, S. & Jayaraman, V. SnO_2: a comprehensive review on structures and gas sensors. *Prog. Mater. Sci.* **66**, 112–255 (2014).
45. Jung, G. et al. A low-power embedded poly-Si micro-heater for gas sensor platform based on a FET transducer and its application for NO_2 sensing. *Sens. Actuators B Chem.* **334**, 129642 (2021).
46. Jung, G. et al. Innovative gas sensing method using transient behavior of FET-type sensors with gate pulse input. In *Proc. Technical Digest - International Electron Devices Meeting, IEDM* Vols 2022 (IEEE, 2022).
47. Swenson, H. & Stadie, N. P. Langmuir's theory of adsorption: a centennial review. *Langmuir* **35**, 5409–5426 (2019).
48. Prezioso, M. et al. Training and operation of an integrated neuromorphic network based on metal-oxide memristors. *Nature* **521**, 61–64 (2015).
49. Ham, D., Park, H., Hwang, S. & Kim, K. Neuromorphic electronics based on copying and pasting the brain. *Nat. Electron.* **4**, 635–644 (2021).
50. Demasius, K. U., Kirschen, A. & Parkin, S. Energy-efficient memcapacitor devices for neuromorphic computing. *Nat. Electron.* **4**, 748–756 (2021).
51. Marković, D., Mizrahi, A., Querlioz, D. & Grollier, J. Physics for neuromorphic computing. *Nat. Rev. Phys.* **2**, 499–510 (2020).
52. Northcutt, C., Jiang, L. & Chuang, I. Confident learning: estimating uncertainty in dataset labels. *J. Artif. Intell. Res.* **70**, 1373–1411 (2021).
53. Northcutt, C. G., Athalye, A. & Mueller, J. Pervasive label errors in test sets destabilize machine learning benchmarks. In *Proc. Advances in Neural Information Processing Systems* (NeurIPS, 2021).
54. Li, P. et al. CleanML: a study for evaluating the impact of data cleaning on ML classification tasks. In *Proc. International Conference on Data Engineering*, Vols 2021 (IEEE, 2021).
55. Casaburi, A., Piombino, P., Nychas, G. J., Villani, F. & Ercolini, D. Bacterial populations and the volatilome associated to meat spoilage. *Food Microbiol.* **45**, 83–102 (2015).
56. Allegrini, F. & Olivieri, A. C. IUPAC-consistent approach to the limit of detection in partial least-squares calibration. *Anal. Chem.* **86**, 7858–7866 (2014).

Author contributions

Gyuweon Jung conceived the idea, performed the experiments, and wrote the manuscript. Gyuweon Jung and Jaehyeon Kim performed the machine learning simulations. Gyuweon Jung, Kangwook Choi, Hunhee Shin, Jinwoo Park, and Donghee Kim fabricated the devices and sensors. Kwon Dongseok, Wonjun Shin, Jangsaeng Kim, Ryun-Han Koo, and Woo Young Choi contributed to data validation and manuscript review. Jong-Ho Lee supervised the project. All authors discussed the results and commented on the manuscript.

Funding

This work was supported by the BK21 FOUR program of the Education and Research Program for Future ICT Pioneers, Seoul National University; the New Faculty Startup Fund from Seoul National University and SNUTI Research Startup for New Faculty of School of Transdisciplinary Innovations, Seoul National University; the National Research Foundation of Korea (NRF) grant funded by the Korea government (MSIT) (RS-2025–00517999).

Competing interests

The authors declare no competing interests.

Additional information

Supplementary information The online version contains supplementary material available at https://doi.org/10.1038/s41467-026-76918-1.

Correspondence and requests for materials should be addressed to Jong-Ho Lee.

Peer review information *Nature Communications* thanks Seong Chan Jun, Mahesh Kumar, and the other anonymous reviewer(s) for their contribution to the peer review of this work. A peer review file is available.

Reprints and permissions information is available at http://www.nature.com/reprints

Publisher's note Springer Nature remains neutral with regard to jurisdictional claims in published maps and institutional affiliations.

Open Access This article is licensed under a Creative Commons Attribution-NonCommercial-NoDerivatives 4.0 International License, which permits any non-commercial use, sharing, distribution and reproduction in any medium or format, as long as you give appropriate credit to the original author(s) and the source, provide a link to the Creative Commons licence, and indicate if you modified the licensed material. You do not have permission under this licence to share adapted material derived from this article or parts of it. The images or other third party material in this article are included in the article's Creative Commons licence, unless indicated otherwise in a credit line to the material. If material is not included in the article's Creative Commons licence and your intended use is not permitted by statutory regulation or exceeds the permitted use, you will need to obtain permission directly from the copyright holder. To view a copy of this licence, visit http://creativecommons.org/licenses/by-nc-nd/4.0/.

© The Author(s) 2026